UCRL 6470

UNIVERSITY OF
CALIFORNIA

Ernest O. Lawrence

Radiation Laboratory

PROTON CAPTURE GAMMA RAYS FROM Si^{28} IN THE REGION OF THE PHOTONUCLEAR GIANT RESONANCE

LIVERMORE SITE

DISCLAIMER

UCRL-6470
Physics, UC-34
TID-4500 (16th Ed.)

UNIVERSITY OF CALIFORNIA

Lawrence Radiation Laboratory

Livermore, California

Contract No. W-7405-eng-48

PROTON CAPTURE GAMMA RAYS FROM Si^{28} IN THE REGION OF THE PHOTONUCLEAR GIANT RESONANCE

Calvin C. Gardner

(Ph. D. Thesis)

May 6, 1961

Printed in USA. Price $1.00. Available from the Office of Technical Services, Department of Commerce, Washington 25, D. C.

PROTON CAPTURE GAMMA RAYS FROM Si^{28} IN THE REGION OF THE PHOTONUCLEAR GIANT RESONANCE

Contents

Contents (Continued)

PROTON CAPTURE GAMMA RAYS FROM Si^{28} IN THE REGION OF THE PHOTONUCLEAR GIANT RESONANCE

Calvin C. Gardner

Lawrence Radiation Laboratory

University of California

Livermore, California

May 6, 1961

ABSTRACT

The Livermore 90-inch variable-energy cyclotron was used to measure the 90° excitation function for the $Al^{27}(p, \gamma)Si^{28}$ reaction. Proton energies between 5 and 13 Mev were used which gave excitation energies in Si^{28} corresponding to the region of the photonuclear giant resonance. Two gamma rays were observed: γ_0, the ground-state gamma ray and γ_1 resulting from deexcitation through the first excited state of Si^{28} at 1.78 Mev. They were detected by a 5-in.-diam by 6-in.-long NaI(Tl) crystal. A Pb collimator was used to improve the resolution of the detector. The results indicate that both γ_0 and γ_1 display the giant resonance behavior; the γ_0 curve reaches a peak value of ~8 μbarns/sr at E_p = 8.75 Mev, while the γ_1 peak is ~14 μbarns/sr at E_p = 10 Mev. Both curves display the fine structure previously reported by Gove et al.[1] A detailed balance calculation was made, using the γ_0 data. A comparison with the measurements of Johansson[2] on the total yield of protons from the $Si^{28}(\gamma, p)Al^{27}$ reaction indicates that about 1/3 of the total photoproton production in Si^{28} results in maximum energy, or ground-state protons. It is concluded that this large proportion strongly suggests a direct interaction reaction mechanism.

I. INTRODUCTION

A. The Nuclear Photoeffect and the Giant Resonance

The many studies made in recent years of the interaction of photons with nuclei, have proven to be quite fruitful.[3] Investigations of radiative transitions in the lighter nuclei, for example, have demonstrated the governing action of the isotopic spin selection rules, and thus the applicability of the principle of the charge independence of nuclear forces.[4] Other studies, concerned with the photodisintegration of the deuteron, have led to information about the nucleon-nucleon potential.[5]

A major part of the work in this field, however, has centered about the photonuclear giant resonance. This phenomenon appears as a resonant peak in the photon absorption cross section at gamma energies between 14 and 24 Mev, the peak position (E_m) changing with A about as $80A^{-0.27}$. Departures from this smooth variation are observed for the light nuclei. The resonances are found to have a width of from 3 to 7 Mev, with peak cross sections of the order of 100 millibarns.[6, 7, 8]

Due to the lack of a variable energy source of monoenergetic photons, most of the experimental work in the giant resonance region has used as a source of gamma rays the bremsstrahlung spectrum from an electron accelerator. Because of the continuous nature of this spectrum, quantitative results can only be obtained by a rather elaborate unfolding procedure[9] which leaves details of the resonance behavior somewhat uncertain. In spite of this difficulty, however, much information of a general character has been obtained.

The predominantly electric dipole nature of the giant resonance, for instance, has been established[10] by comparisons of the gamma absorption cross section, integrated over the resonance curve (σ_{int}), with the electric dipole sum rule.[11] This model-independent relation, derived by Bethe and Levinger from the similar Reiche-Kuhn atomic sum rule, predicts that $\sigma_{int} \tilde{=} 0.015A$ Mev-barns. Although the effects of higher multipole transitions have been observed, it has been found that for most elements the experimentally determined σ_{int} effectively exhausts this sum.[8, 10]

B. Theory

1. Collective Model

The collective model of Goldhaber and Teller was an early theoretical attempt to explain the mechanism of the giant resonance.[12] This model pictures the nucleus as composed of neutron and proton fluids, and the resonance as a bulk oscillation of these fluids within the nuclear volume. The result is a linear oscillation of the center of charge about the center of mass, which conforms with the established E1 nature of the resonance. If the envelope of the nucleus is assumed to remain fixed and the fluids to oscillate in such a fashion that their combined density at every point remains constant, then this model predicts that $E_m \propto A^{-1/3}$, which is in fair agreement with experimental results. More quantitative predictions are difficult to obtain from this model, however, since it applies only to the absorption mechanism and says nothing of the decoupling of the oscillation leading to decay of the system.[13]

2. Shell Model

A more recent theoretical approach to this subject has been in terms of the independent particle, or shell, model.[14, 15] Through the work of Wilkinson and others,[16] a simple model has been developed which has been able to explain the general features of the resonance and is in most cases in agreement with available experimental results.[13] In contrast to the collective model, it makes definite predictions about decay mechanisms, and is thus more useful for comparison with experiment.

The tendency of E1 transitions to cluster in such a fashion as to form the giant resonance can be understood in terms of the independent particle model by considering first the simplest shell model, the isotropic harmonic oscillator. The clustering then follows from the equal spacing of levels in the oscillator potential and the selection rule for E1 transitions allowing only transitions between adjacent levels. In the more realistic finite square-well potential, this equal spacing is apparently lost. However, levels of a given sequence, such as 1s, 1p, 1d, ... or 2s, 2p, 2d, ... , are still almost equally spaced, at least near the Fermi surface.[15] Furthermore, the transitions between such levels of a given sequence, which were the allowed transitions in the harmonic oscillator potential, are now favored transitions. This is seen in Table I which gives the square of the radial overlap integrals for various transitions. Since the Pauli principle restricts the absorption to those nucleons within one oscillator spacing of the Fermi surface, it is apparent that photons with energy nearly equal to this oscillator spacing can be absorbed in a resonant fashion, raising a nucleon near the Fermi surface to an unfilled single particle level, preferably of the

Table I. Radial overlap integrals for an infinite square well.* (D is the square of the radial overlap integral measured in units of the nuclear radius.)

$1(\ell)$ to $1(\ell+1)$	ℓ	0	1	2	3	4	5	6
	D	0.28	0.38	0.44	0.49	0.53	0.56	0.58

$2(\ell)$ to $2(\ell+1)$	ℓ	0	1	2	3
	D	0.23	0.28	0.33	0.37

$3(\ell)$ to $3(\ell+1)$	ℓ	0	1
	D	0.22	0.25

$1(\ell)$ to $2(\ell-1)$	ℓ	1	2	3	4	5
	D	0.09	0.07	0.05	0.04	0.04

$1(\ell)$ to $2(\ell+1)$	ℓ	0	1	2	3
	D	0.001	0.002	0.002	0.003

$2(\ell)$ to $3(\ell-1)$	ℓ	1	2
	D	0.12	0.09

*D. H. Wilkinson, Physica 22, 1039 (1956).

next higher ℓ value. The width of the giant resonance thus appears as a measure of the clustering of the allowed dipole transitions, which do not all occur at precisely the same energy.

The single particle transition strengths given above must be modified further by the factors of Table II, listed for the various

Table II. Strength of transitions from closed shells in terms of the transition strength for a single particle.*

Transition	S
$\ell + 1/2 \rightleftharpoons \ell + 1 + 1/2$	$\frac{(\ell+1)(\ell+2)}{2\ell+3}$
$\ell + 1/2 \rightleftharpoons \ell + 1 - 1/2$	$\frac{\ell+1}{(2\ell+3)(2\ell+1)}$
$\ell - 1/2 \rightleftharpoons \ell + 1 - 1/2$	$\frac{\ell(\ell+1)}{2\ell+1}$

*D. H. Wilkinson, Physica 22, 1039 (1956).

transitions allowed in jj coupling. These must be applied to transitions from a closed shell, which may be several times stronger than a single particle transition, due to correlations between the equivalent particles of the closed shell.[13] These strengths S are given in terms of the individual transition strengths and depend only upon ℓ. They account for the ability of the independent particle transitions to effectively exhaust the dipole sum rule.[13]

The remaining important consideration in the independent particle model description of the giant resonance is the absolute energy at which the transitions take place. This calculation has been done by Wilkinson and also by Rand[16] and is summarized in a review article by Wilkinson.[13] The calculations draw upon results of recent optical model studies for determination of the radius of the square well, $r = 1.2 \times 10^{-13} A^{1/3}$ cm, and in the use of a velocity-dependent real potential. For nucleons near the Fermi surface, this velocity dependence of the well depth can be

interpreted as an effective mass $m^* \neq m$, which is chosen to be $m^* = m/2$ as is suggested by the Brueckner treatment of nuclear matter. With these considerations, the calculated values of E_m are in fair agreement with experimental results. Wilkinson has shown that a more realistic potential, with a rounded edge, would tend to strengthen the agreement. It is emphasized that the ability of the independent particle model to explain the photonuclear giant resonance leans heavily upon the concept of an effective mass.[13]

An alternative explanation that has recently been suggested[17] relies upon the collective nature of the closed shells which contribute the bulk of the dipole strength. This approach takes into account the particle-hole interaction involved in the single particle transition from a closed shell. It is found that due to the $T = 1$ nature of the intermediate state (required by the isotopic spin selection rule for E1 transitions) this particle-hole interaction is strongly repulsive, which tends to increase the energy of the intermediate state. This improvement should allow a more quantitative comparison between theory and experiment.

C. Photonuclear Reactions

In addition to offering an explanation of the total absorption of gamma radiation, the independent particle model suggests a simple picture of the photoproduction reaction mechanism in the giant resonance region. The model pictures a specific absorption transition as raising a nucleon to a single particle state, from which it may decay directly (width Γ), or through the action of the imaginary potential be amalgamated into a compound nucleus which decays by some statistical

mode. If the width for the latter possibility is designated as 2W (W is the depth of the imaginary potential) and if the cross section for the specific absorption transition is σ', then the direct reaction cross section is given by $\sigma = \sigma'(\Gamma/2W)$. This resonance direct emission is similar to the early direct emission of Courant[18] which, however, gave cross sections which were too low due to the neglect of resonance effects. σ' can easily be found, using Tables I and II, by comparing the transition strength of the initial transition picked out by the reaction with the total absorption transition strength found by weighting and summing all possible transitions for the nucleus in question. This fraction of the total absorption cross section then equals σ'. This picture is, of course, only a first-order model.

D. Ground-State Reactions

Those photonuclear reactions which leave the final nucleus in its ground state are especially interesting for two reasons. (1) Ground-state decays by a statistical mode are improbable. Thus if an appreciable number of ground-state photoneutrons or photoprotons are observed they can almost certainly be interpreted as the products of some form of direct interaction. (2) The ground-state reaction can be reached by means of the inverse reaction, in which a nucleon is captured and a ground-state gamma ray results. The principle of detailed balance relates the capture and photoproduction cross sections.

E. Purpose of this Investigation

This paper presents the results of a study of the $Al^{27}(p, \gamma)Si^{28}$ reaction in the region of the photonuclear giant resonance. In order

to facilitate comparison with theoretical reaction mechanisms, care was taken to obtain absolute cross sections. The 90° excitation function was measured over the entire resonance region. In addition, an angular distribution was obtained at E_p = 8.7 Mev. Aluminum was chosen as the bombarded element because of the availability, ease of foil preparation, and isotopic purity of this element, and the general success of shell model calculations in this region of the periodic table. In addition, the closing of the $d_{5/2}$ subshell at Si^{28} suggests that resonance direct emission of ground-state nucleons should be especially strong for this nucleus.

II. METHOD

A. General Description

The experiment was done at Livermore, using the 90-inch variable-energy cyclotron as a source of protons. Figure 1 is a photograph and Fig. 2 a schematic diagram of the experimental arrangement. The beam from the cyclotron was focused through a collimator onto the foil and then collected in a long Faraday cup. The detector was mounted on an angle changer, with the crystal face 16 in. from the foil center. It is shown positioned at 90° to the beam line.

The foils were mounted on a foil rack and changer mechanism, and were selected and positioned from the control room. The rack included a blank which was used for background measurements, and a plastic foil which, when inserted into the beam, served as a source of 4.43-Mev gamma rays. These originate from inelastic scattering of the incident particles off carbon nuclei within the plastic, and were used, in conjunction with a tail pulser, to calibrate the energy of the γ spectrum. Aluminum foils of about 20 mg/cm^2 were used, which give an energy width of about 1/2 to 1 Mev, for the range of incident particle energies used in the experiment. The exact foil thicknesses are given in Table III.

B. Faraday Cup

The current-collecting cup was designed with the following considerations in mind.

(1) Because of Coulomb scattering from nuclei within the foil, the beam of incident charged particles is essentially defocused at that point. In order to obtain an accurate current reading, the cup, as seen

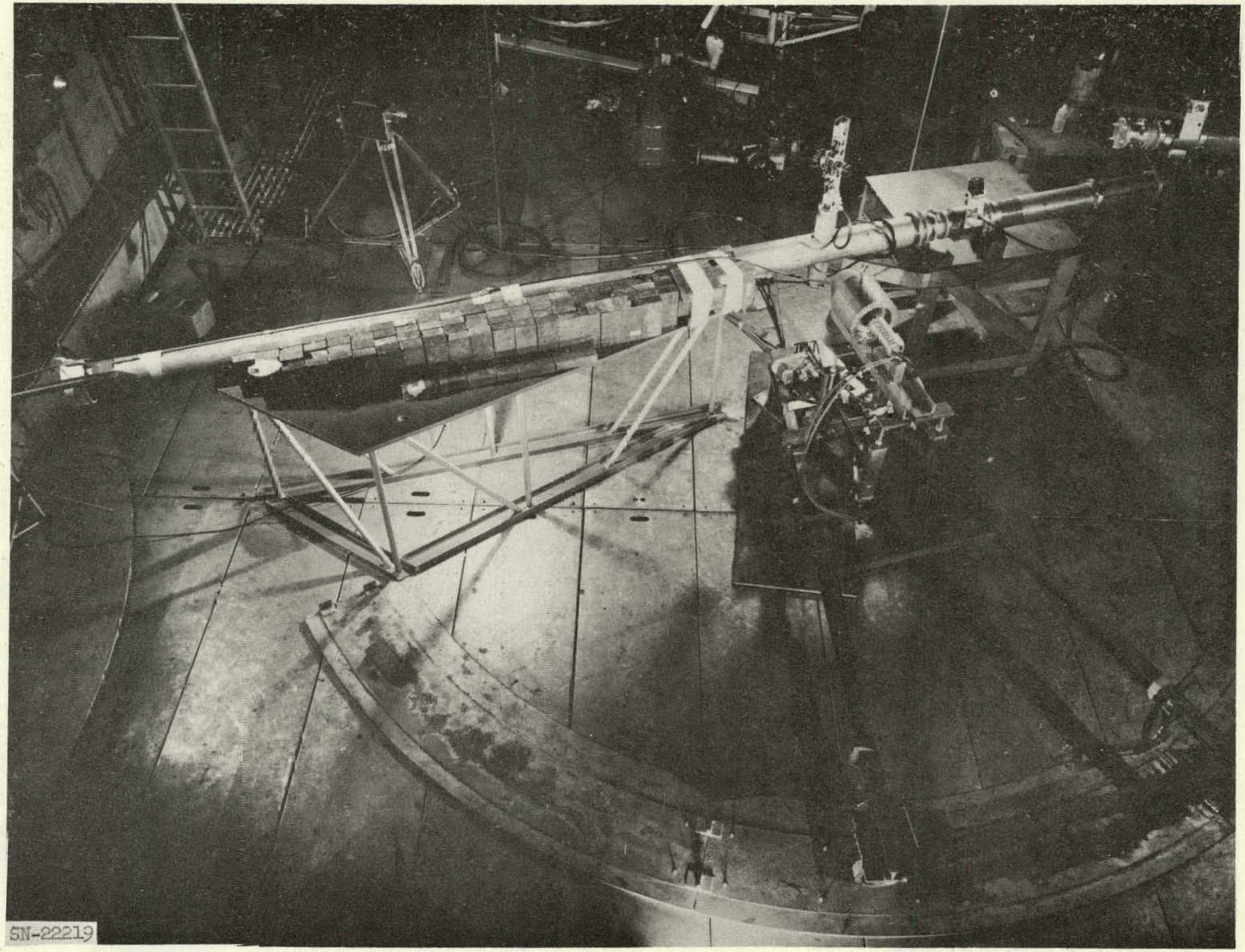

Fig. 1. Photograph of experimental setup.

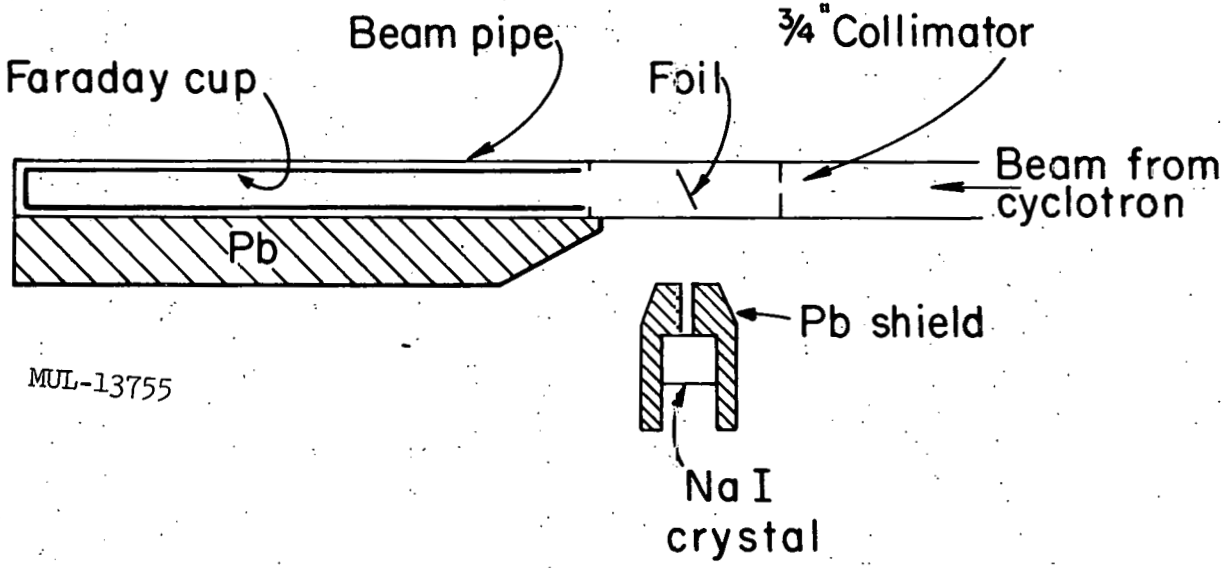

Fig. 2. Experimental geometry. (Not to scale)

from the foil, must subtend as large a solid angle as possible. With an entrance aperture of 5 in. placed 20 in. from the foil, the fraction of incident particles scattered into angles large enough to miss the cup was calculated to be less than 1.5%. Since larger errors are assigned to the data for other reasons, no correction has been made for this effect.

(2) The cup, acting as a beam stopper, was a source of background. With the design as shown in Fig. 2, most of the beam is collected at the rear of the cup and is shielded from the detector by a long path of lead. Carbon was chosen as the cup material because of the high ($\sim$18 Mev) $C^{12}(p,n)N^{12}$ threshold. The background radiation reaching the detector from this source was measured for various incident particle energies and found to be sufficiently low, with the design as shown. It consisted almost entirely of the 4.43-Mev inelastic γ ray from C^{12}. The effect of neutrons created in the $C^{13}(p,n)N^{13}$ reaction was not noticeable. The charge collected in the cup was measured by a current integrator, and recorded for each run.

C. Gamma Detectors

Two detectors were used in the course of the experiment. The first, diagrammed in Fig. 3, consisted of a 4-in.-diam by 4-in.-long NaI(Tl) crystal, viewed by a Dumont 6363 photomultiplier. A light-reflecting disk of Teflon was placed against the crystal face, around the photocathode of the photomultiplier tube. The unit was placed in a light-tight cylinder, which also served to hold the photomultiplier in position and was wrapped with a magnetic shielding material. The detector was placed in a lead shield, 2 in. thick around the crystal,

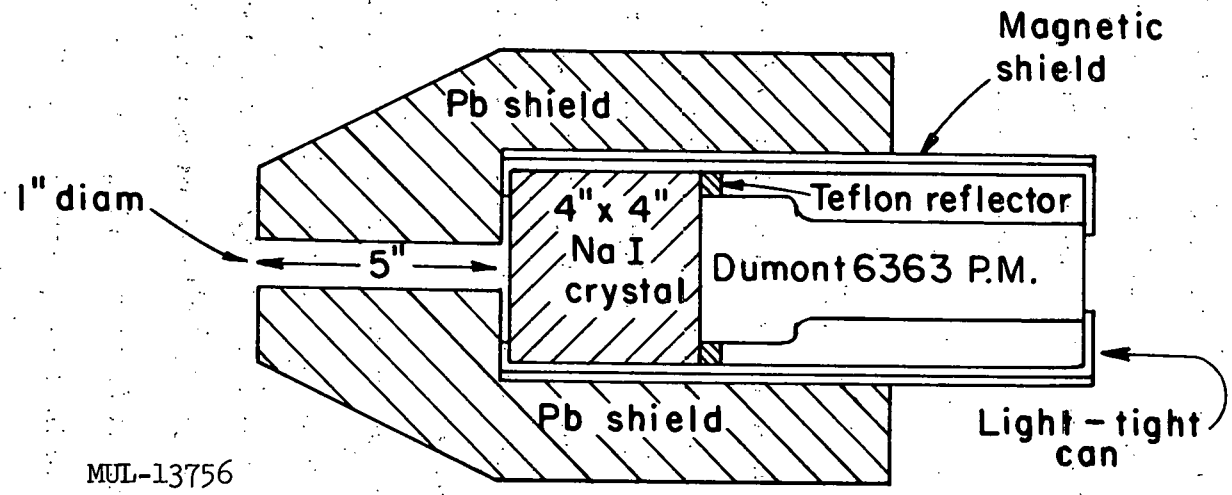

Fig. 3. First detector with Pb collimator.

and formed into a collimator in front of the crystal, as shown. The shield reduced background, and by collimating the γ rays along the axis of the crystal, reduced edge effects and bremsstrahlung losses, improving the resolution of the detector. (See Fig. 6.)

The second detector was obtained from Harshaw Co. in time for the final data-taking run. It consisted of a 5-in.-diam by 6-in.-long NaI(Tl) crystal and Dumont 6363 photomultiplier in a "matched-window" assembly.[19] This design gives better resolution for large crystals. It was also used in a similar Pb shield.

D.- Electronics

A block diagram of the detector electronics is given in Fig. 4. After initial amplification by the preamplifiers, pulses from the detector were shortened to 0.5 μsec by a clipping line, which was placed in the control room for convenience. The pulse-height spectrum was then passed through a discriminator, amplified, and displayed on an Argonne type pulse-height analyzer.

It was found necessary to use three preamplifiers in order to obtain pulse heights sufficient for operation of the biasing diode, or discriminator. Care was taken to operate the preamplifiers below saturation. The adjustable discriminator was used to keep pulses below the region of interest from reaching the pulse-height analyzer.

A major problem in the experiment was the elimination of "pile-up" pulses from the spectrum. These are caused by the coincident arrival at the crystal of several low-energy photons or neutrons, which can add together to give an apparent high-energy pulse. The detector was exposed to a relatively intense flux of low-energy photons and

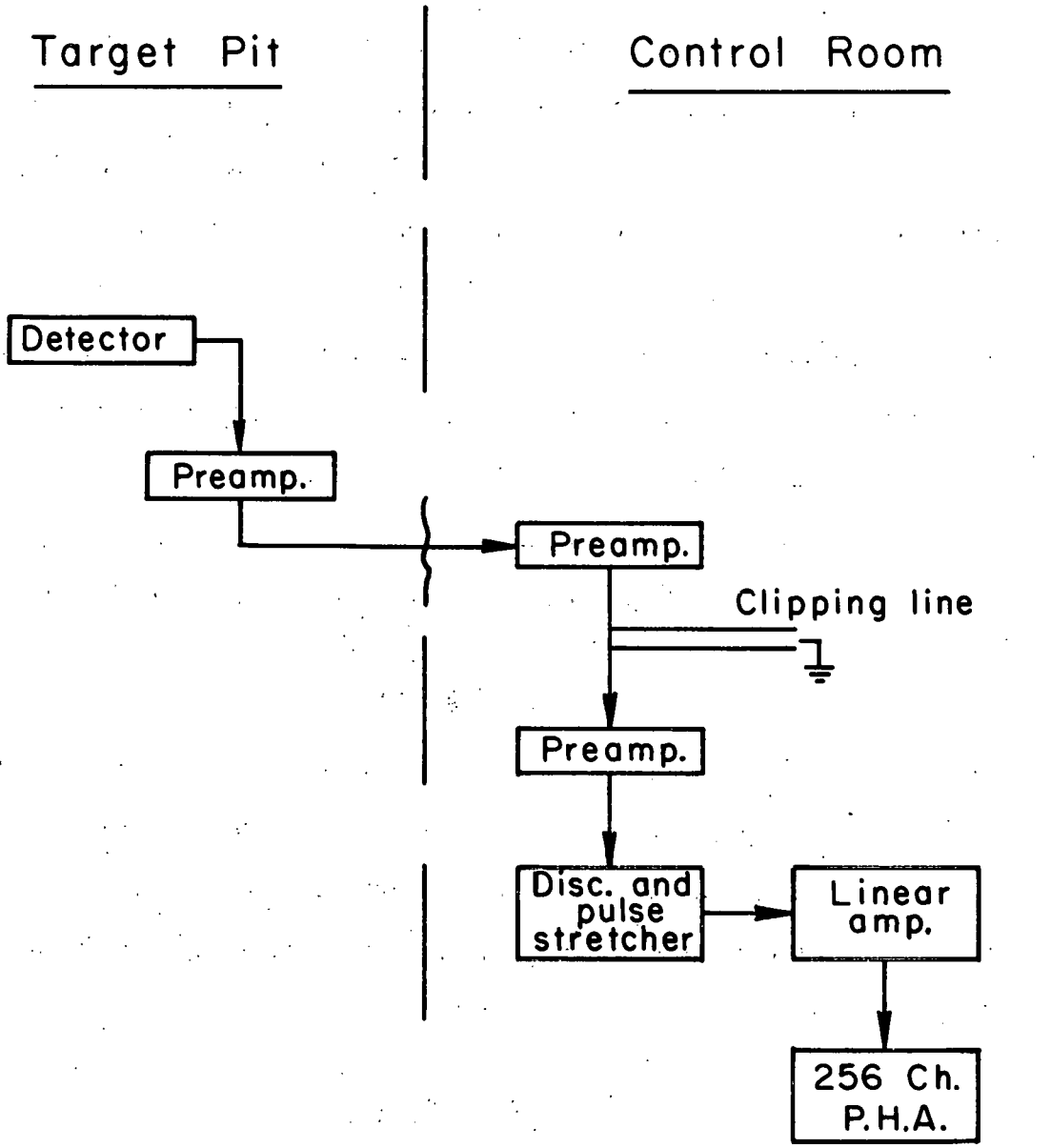

Fig. 4. Electronics block diagram.

neutrons which originated in the beam stopper, the collimator, and the foil itself. By removing the foil, it was determined that the greater part of this background was due to the interaction of the incident particles with nuclei within the foil. These interactions can take the form of inelastic collisions with the subsequent emission of a deexcitation gamma ray, or, at the higher energies used in this experiment, of neutron production. In either case, photons or neutrons are produced which, when captured in the crystal, produce a low-energy pulse. The piling up of these small pulses can be minimized by reducing the pulse length by means of the clipping line, and by decreasing the current of incident particles, i.e., spreading out the pulses over a longer time interval. It was found that with a pulse length of 0.5 μsec, a proton current of 0.05 to 0.1 μa produced no pile-up counts in the spectrum.

E. Background

Above $E_\gamma \tilde{=}$ 15 Mev, the only background was found to be due to cosmic radiation. Measurements with the foil out showed that it was independent of the beam and of E_γ. It was equal to 1.68 counts/min-Mev for the first detector, and 2.31 counts/min-Mev for the larger detector.

F. Observed Spectra

A typical pulse-height spectrum is reproduced in Fig. 5, and shows two gamma rays: the ground-state gamma ray γ_0, and the gamma ray γ_1 resulting from deexcitation through the first excited state of Si^{28} at 1.78 Mev.

The detector electronics was found to be linear, by a measurement of pulser voltage vs channel number. Thus a comparison of

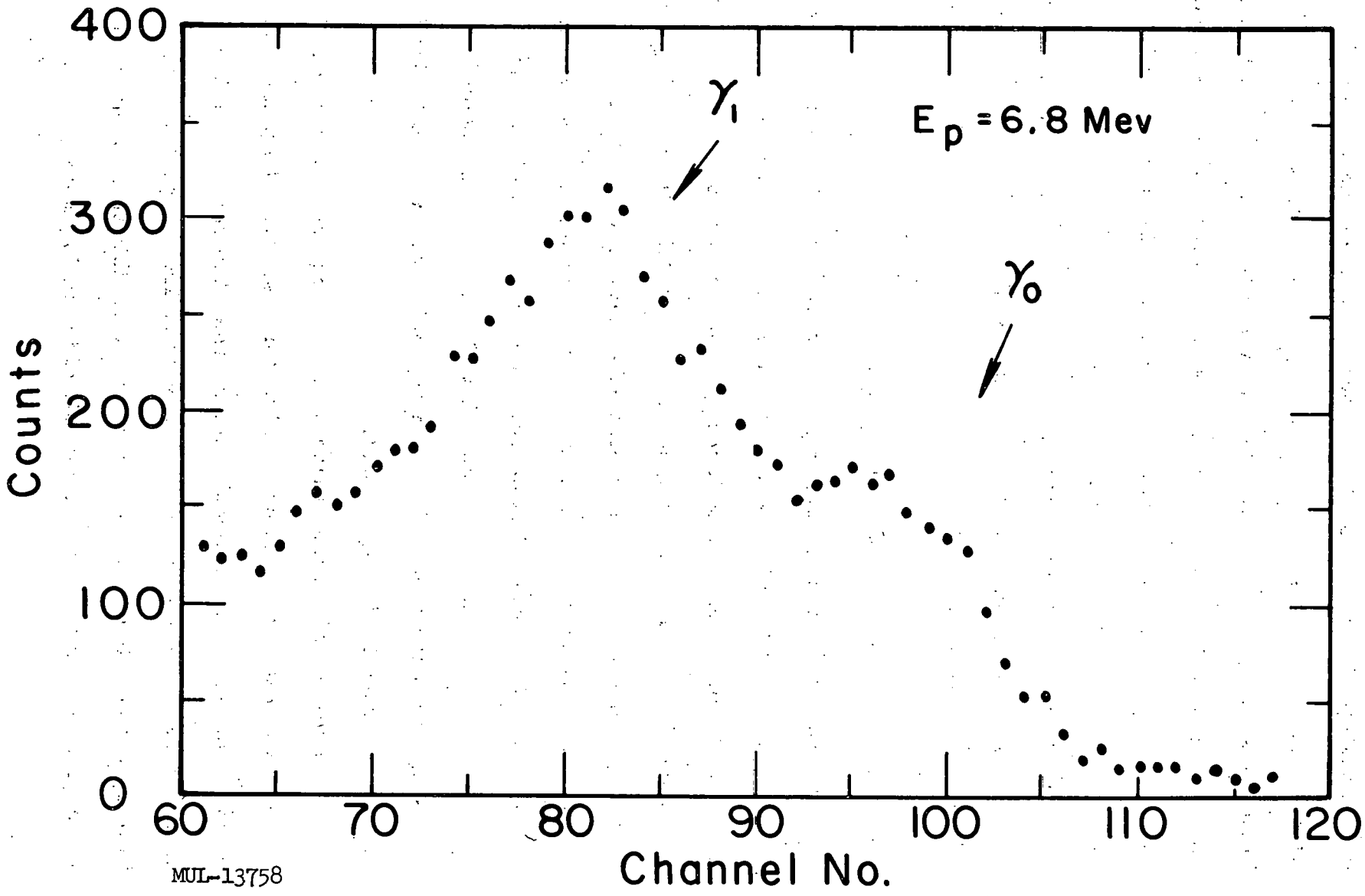

Fig. 5. Typical spectrum (5 in. × 6 in. crystal).

pulser voltages for the 4.43-Mev carbon γ ray and either γ_0 or γ_1 determined an energy scale. E_{γ_0} and E_{γ_1} are known from the reaction kinematics (i.e., $E_{\gamma_0} = \frac{27}{28} E_p + 11.6$ Mev and $E_{\gamma_1} = E_{\gamma_0} - 1.78$ Mev). Since the gamma peak position cannot be determined exactly, an error exists in the energy calibration. This uncertainty is taken into account in the data reduction procedure.

The statistics on most runs were about as shown in Fig. 5. Usually ~ 100 counts/channel were obtained over the γ_0 peak in about 30 minutes running time.

G. Line Shape

In order to interpret properly the observed spectra, a measurement was made of the line shape, i.e., the pulse-height spectrum of the detector for a monoenergetic γ ray of the appropriate energy. A convenient source of 19.8-Mev photons was available from the $H^3(p,\gamma)He^4$ reaction, using the Livermore Cockcroft-Walton accelerator as a source of protons. A tritium-loaded titanium target was used. The proton energy was 350 kev which is well below the threshold for all competing reactions; thus the source is reasonably clean, and appropriate for a line-shape measurement. The geometry and electronics were identical to those used in the experiment.

The results of the line-shape measurement are shown in Fig. 6. The general features are interpreted as follows. (1) The main peak is composed of two unresolved peaks. The shoulder on the upper energy side represents the full energy peak and the peak displaced down by 1/2 Mev is due to the escape of one annihilation quantum. (2) The asymmetry on the low-energy side of the main peak is due to the

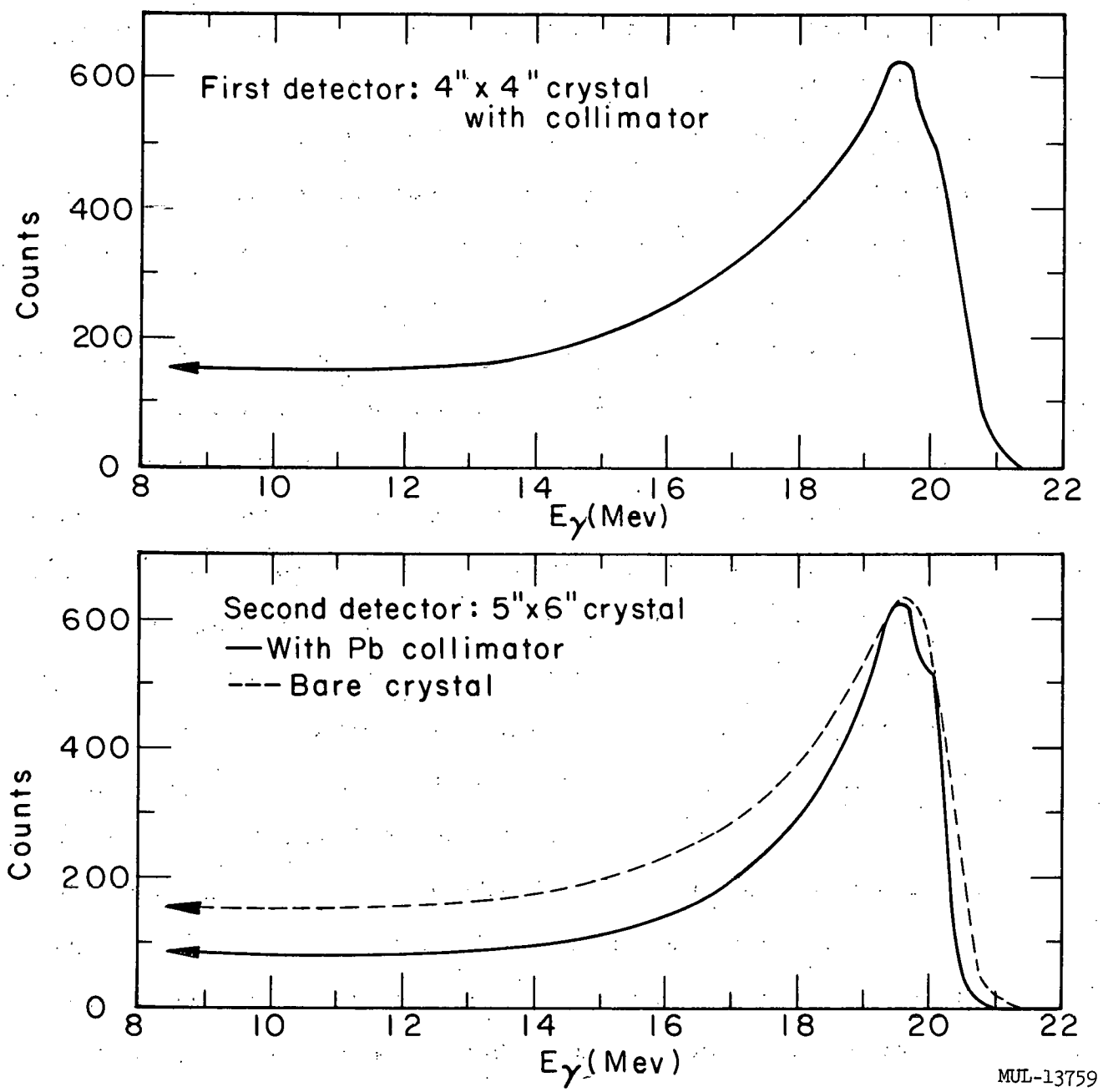

Fig. 6. Line shapes for E_γ = 19.8 Mev.

escape of low-energy bremsstrahlung quanta. (3) The long flat tail is due to Compton scattering and edge effects.

The tail was found to remain flat down to E_γ = 5 Mev for the first detector and 8 Mev for the second detector. Below this energy a rise was observed, which was found to be due to a neutron background, partially beam dependent. The proximity of the cyclotron explains the general background, while the beam-dependent neutrons could be produced by the $d(d,n)He^3$ reaction resulting from deuteron contamination of the proton beam. For purposes of calculating absolute cross sections, the assumption was made that the tail remains flat down to zero energy. The ratio of counts under the extrapolation to total counts was found to be 0.16 for the first detector and 0.24 for the second.

Figure 6 shows the better resolution obtained by the larger crystal in a matched-window assembly. It should be noted, however, that different phototubes were used in each detector and a slightly longer pulse length was used with the second detector. Thus the better resolution may be due partly to the associated electronics.

It is also clear from Fig. 6 that the Pb collimator provides a considerable improvement in resolution. By confining the incoming photons to the axis of the crystal, edge effects at the sides of the crystal are greatly reduced. Bremsstrahlung losses are reduced for the same reason. Energy losses can still occur at the back face of the crystal, however, which accounts in part for the low energy tail.

H. Detector Efficiency

The detector efficiencies are calculated for $E_\gamma = 19.8$ Mev to be $\epsilon_T = 0.81$ for the first detector and $\epsilon_T = 0.91$ for the second, where ϵ_T = no. of γ's detected/no. of γ's incident. The relation $\epsilon_T = 1 - e^{-\mu\xi}$ was used, where ξ is the crystal thickness in g/cm^2 and μ is the mass absorption coefficient. The solid angle Ω(det) subtended by the detector was assumed to be $\Omega_0 F$ where $\Omega_0 = (1/2)^2 \pi/(16)^2$ and F is a factor which corrects for imperfect collimation. Since the complete line shape is used in the data-reduction procedure, it is not necessary to compute a peak efficiency (i.e., the probability that an incident γ gives a count in the peak of the line shape).

The collimation correction factor F was computed from the formula

$$F = 1 + \frac{2\pi}{\Omega_0} \int_{\theta_0}^{\theta_1} \theta\, e^{-\mu' r}\, d\theta,$$

where μ' is the linear absorption coefficient (in.$^{-1}$) in Pb, $\theta_0 = 1/32$, $\theta_1 = 1/22$ and $r = \frac{16}{\cos\theta} - \frac{1}{2\sin\theta}$. This relation was derived from the figure below and represents an increase in the effective solid angle due to photons transmitted through the Pb. The integral was evaluated

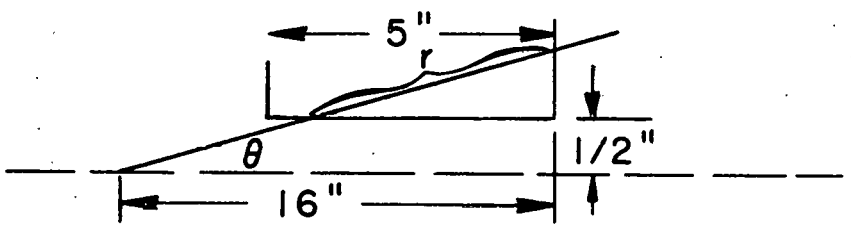

numerically for various values of μ' corresponding to the γ energies detected. $F(E_\gamma)$ is plotted in Fig. 7. No correction was made for inscattering or other secondary effects.

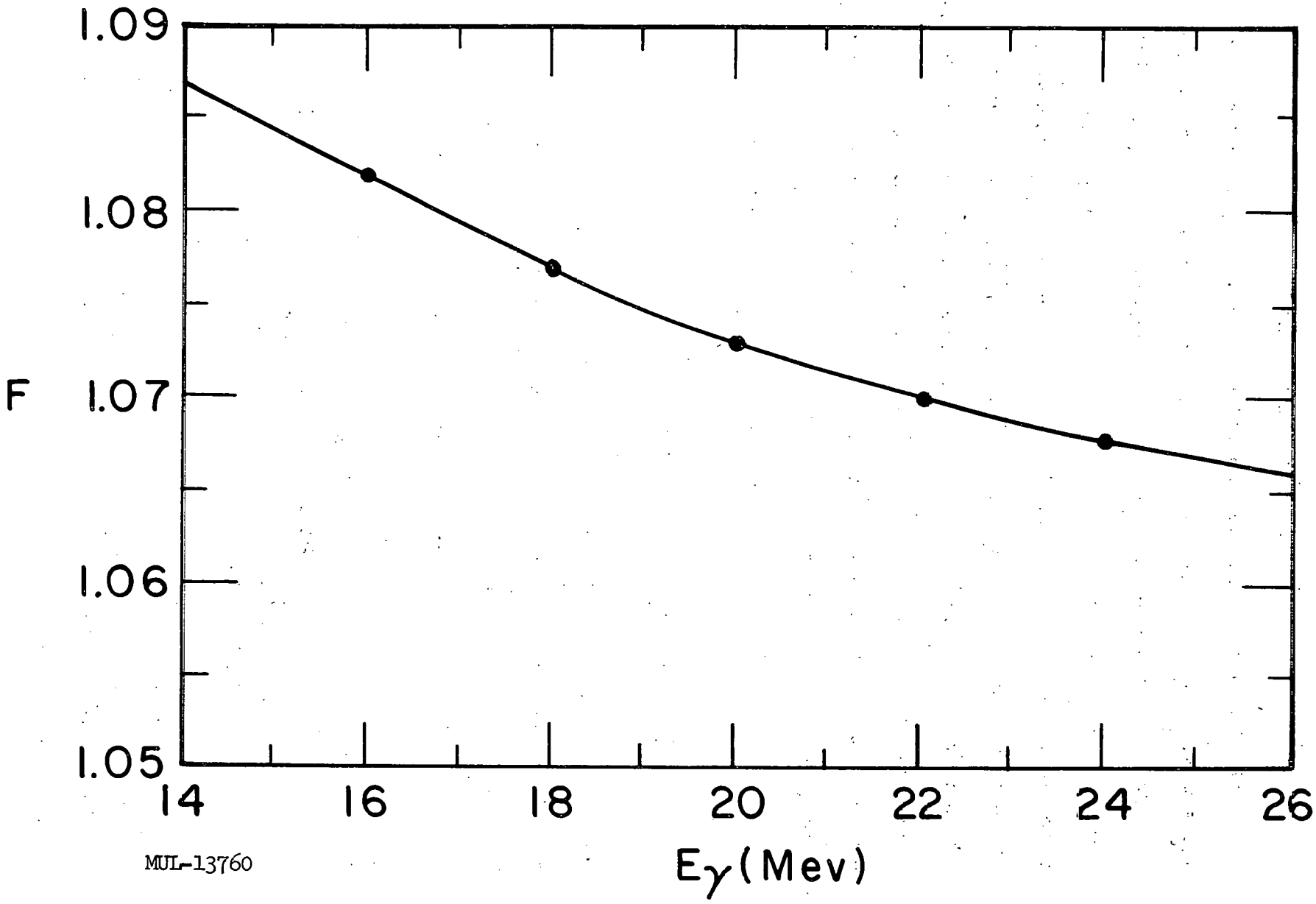

Fig. 7. Collimation correction factor F.

I. Data Reduction

The problem of reducing the measured raw spectra to cross sections with errors, was programmed for the IBM 650 computer at Livermore. The procedure involved the following steps:

(1) An energy scale was put on the spectrum, as previously described. The flat background due to cosmic rays was then subtracted and the resultant spectrum printed out and plotted (see Fig. 9).

(2) Using the line shape measured at 19.8 Mev, a new line shape was then generated for E_{γ_0}. For this purpose the assumption was made that the shape of the curve does not change with energy. The procedure is illustrated in Fig. 8.

(3) A square resolution function with width equal to the energy thickness of the foil was then folded into the line shape. This modified the curve somewhat, as shown in Fig. 8.

(4) This final line shape was then compared with the measured spectrum by summing the counts in the leading edge of both the measured γ_0 and the line shape. The ratio of these spectrum counts to line shape counts is then a measure of the relative cross section σ_0(rel), for production of the ground state γ ray.

(5) σ_0(rel) was used to normalize the line shape, which was then subtracted from the spectrum, leaving a residual spectrum composed of the first excited state γ ray.

(6) Using $E_{\gamma_1} = E_{\gamma_0} - 1.78$ Mev, the above procedure was then repeated for γ_1 (i.e., a new line shape was generated for E_{γ_1}, folded by the foil width, compared with the residual spectrum yielding σ_1, normalized by σ_1 and subtracted from the spectrum.)

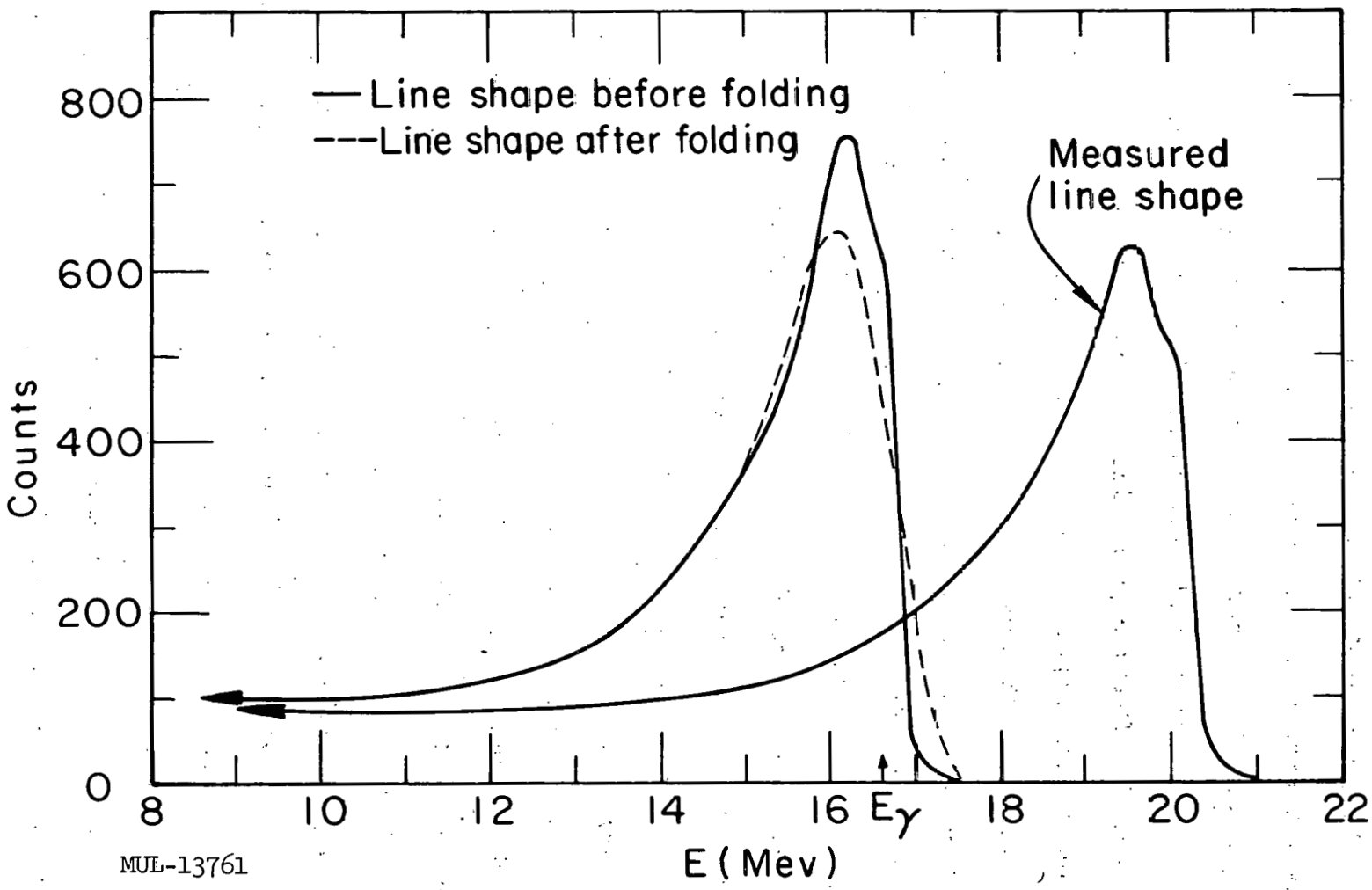

Fig. 8. Folded line shape: 5 in. × 6 in. crystal (1.3-Mev fold width).

The result is a final subtraction spectrum and the cross sections σ_0 (rel) and σ_1 (rel). Since the largest uncertainty in the above procedure was the location of the γ_0 peak (i.e., the absolute energy determination), the process was repeated for channel shifts of -3, -2, -1, +1, +2, and +3. Each of these yields a subtraction spectrum with cross sections. A spectrum and the corresponding family of subtractions are plotted in Fig. 9. The best subtraction curve, then, determines σ_0 and σ_1. The cross sections corresponding to the first curve to either side of this "best" subtraction which is non-zero outside statistics, are a measure of the relative error in σ_0 and σ_1.

For the data of Fig. 9, values of $\sigma_0 = 0.27 \pm 0.03$ and $\sigma_1 = 0.44 \pm 0.04$ were chosen. For most of the data, a one-channel shift was sufficient to produce an unreasonable subtraction; on some of the data, however, a shift of up to 3 channels was necessary, which is reflected in larger relative errors on these points. The errors determined in this fashion were larger, in general, than the statistics on the sum of counts over the leading edge of the measured γ ray.

Good subtractions were obtained over the entire energy range of the gammas (~ 15 to 24 Mev), which implies that the line shape did not change noticeably from the one measured at $E_\gamma = 19.8$ Mev.

Cross sections were finally computed from the formula

$$\frac{d\sigma}{d\Omega}(\theta) = \left[\frac{\bar{A}}{N_0 \rho_A}\right] \frac{n_0 \sigma(\text{rel})}{q \Omega(\text{det}) \epsilon_T(E_\gamma)}$$

where

$\bar{A}$ = atomic number of foil material

N_0 = Avagadro's number

ρ_A = thickness of foil in g/cm^2.

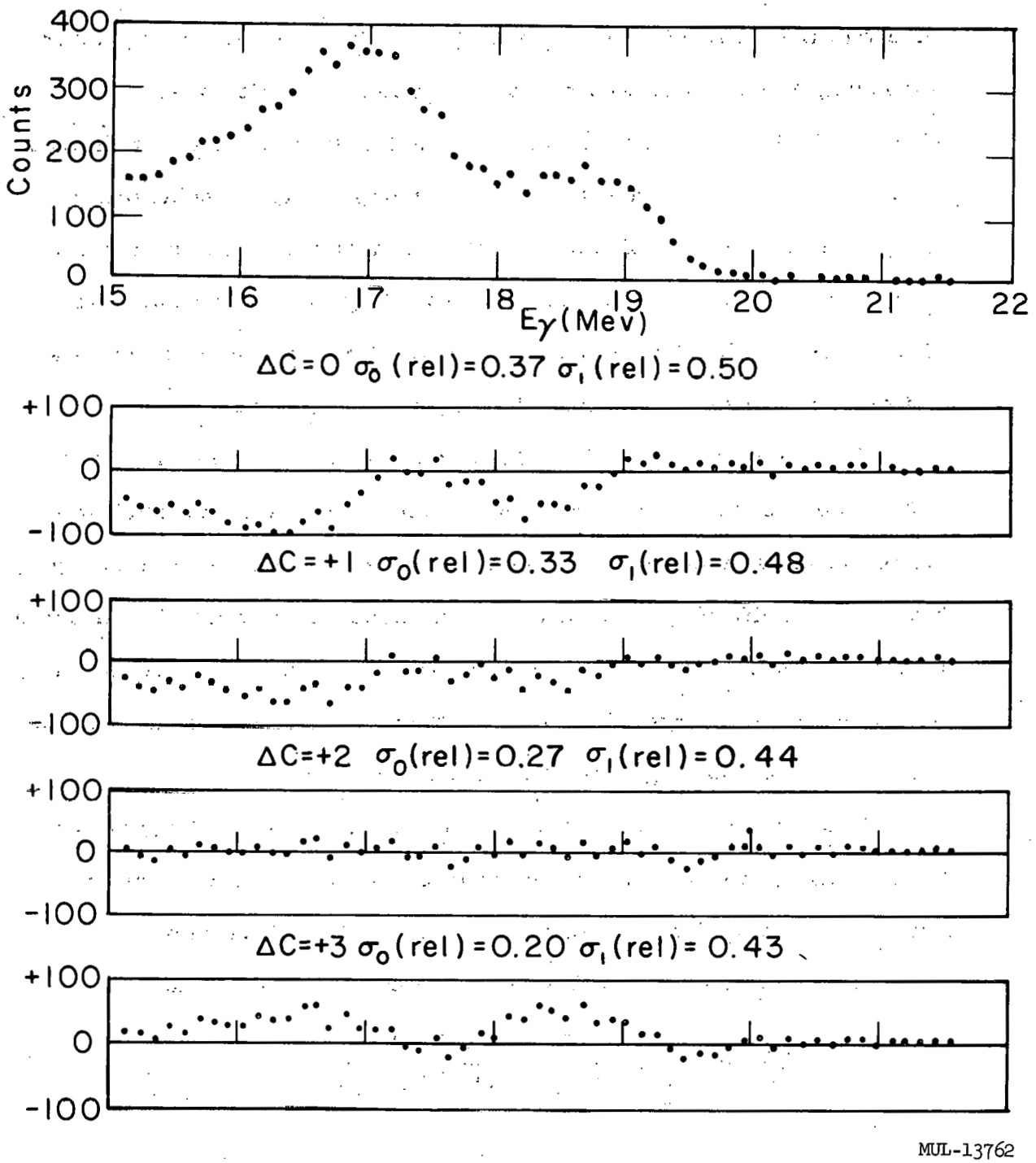

Fig. 9. Spectrum with subtractions for several values of ΔC (channel shift).

q = number of particles incident (proportional to charge collected in cup)

$\Omega(\text{det})$ = solid angle subtended by the detector at the foil

$\epsilon_T(E_\gamma)$ = total efficiency of detector

n_0 = counts in line shape used in computing $\sigma(\text{rel})$.

III. RESULTS

The results are tabulated in Table III and the excitation functions presented graphically in Fig. 10. The gamma-ray angular distributions, measured at a proton energy of 8.7 Mev, are shown in Fig. 11. The angular accuracy on these measurements was ± 5°. The energy thickness of the foil is given for each measurement in Table III and shown as horizontal flags in Fig. 10. The vertical flags represent the relative errors determined by the subtraction procedure.

In addition to the relative errors, an uncertainty exists in the absolute value of the cross sections, arising primarily from the line-shape extrapolation to zero energy. The assumption that the tail remains flat down to zero energy is justified, in part, by calculations[20] of the line shape expected for high-energy gammas in large crystals. They show the tail remaining flat, or decreasing slightly, with decreasing energy. The neglect of secondary effects, such as Compton scattering of incoming photons by the Pb collimator, also introduces an error. If the ratio of 1/2 the area under the extrapolation to the total area of the line shape is used as a measure of the extrapolation error, a value of ± 10% can be assigned to this uncertainty. In view of this and the other assumptions made in computing the cross sections, an overall absolute error of ± 15% would appear to be realistic.

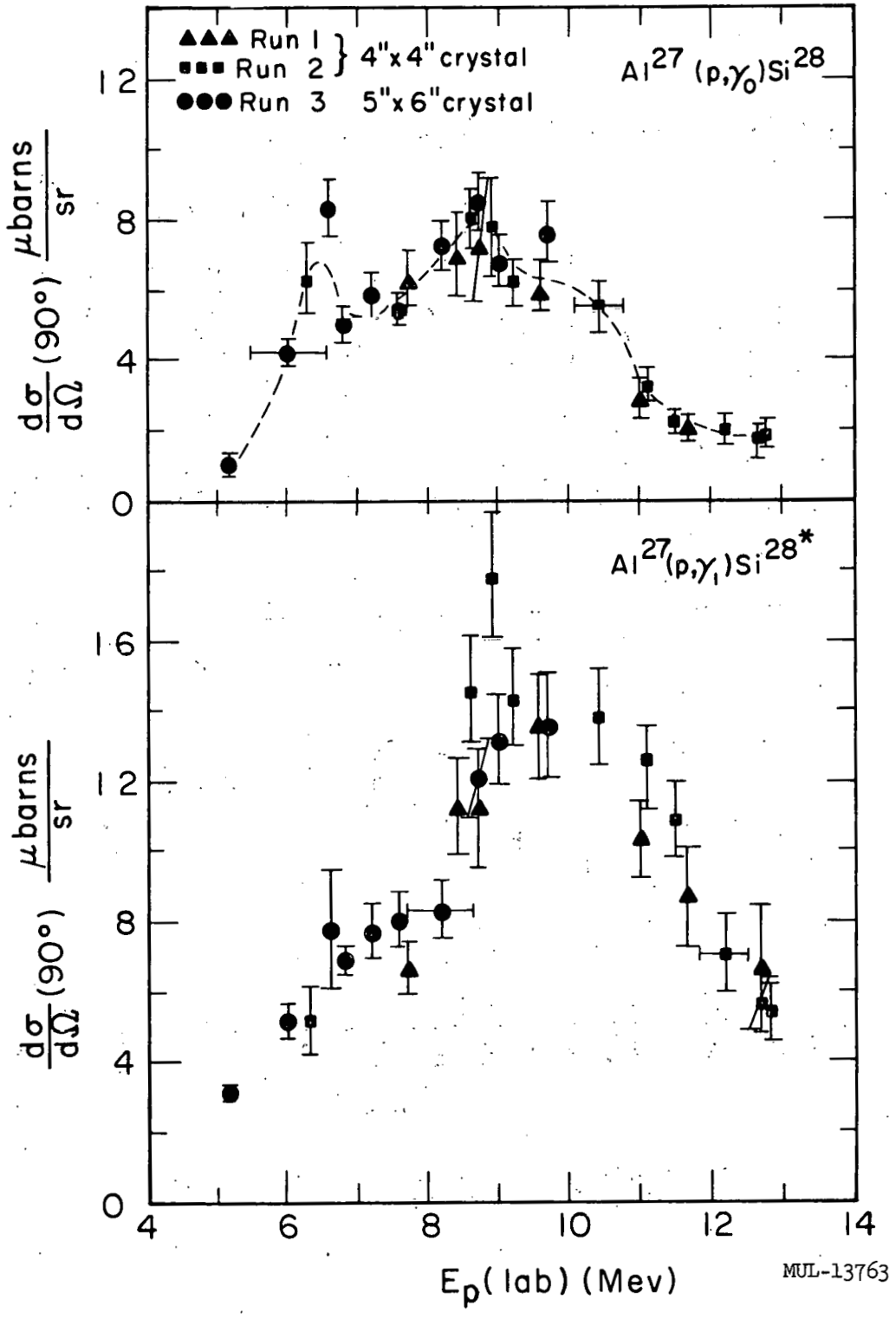

Fig. 10. Measured cross sections.

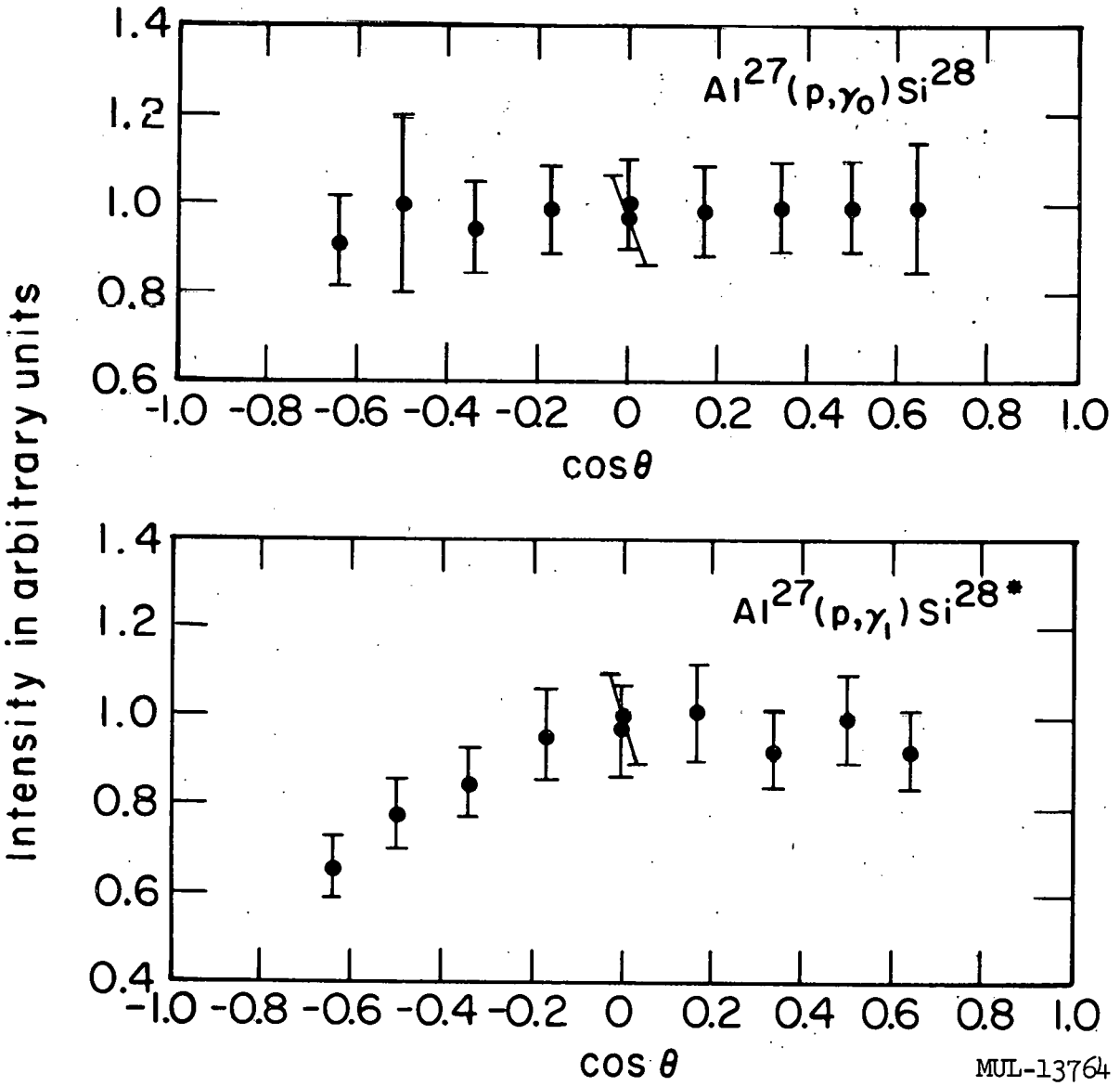

Fig. 11. Measured gamma-ray angular distributions. E_p = 8.7 Mev (ΔE_p = 0.9 Mev). 5 in. × 6 in. crystal.

Table III. Measured 90° cross sections (μbarns/sr).

Run 1: 4×4" crystal
23.05 mg/cm^2 foil

E_p (Mev)	$\frac{d\sigma}{d\Omega}(\gamma_0)$	$\frac{d\sigma}{d\Omega}(\gamma_1)$
7.7 ± 0.5	6.3 ± 0.8	6.6 ± 0.8
8.4 ± 0.45	7.0 ± 1.2	11.2 ± 1.4
8.7 ± 0.45	7.3 ± 1.7	11.2 ± 1.7
9.6 ± 0.4	6.1 ± 0.7	13.5 ± 1.5
11.0 ± 0.35	2.9 ± 0.6	10.2 ± 1.1
11.7 ± 0.35	2.0 ± 0.4	8.6 ± 1.4
12.7 ± 0.35	2.0 ± 0.3	6.5 ± 1.8

Run 2: 4 × 4" crystal
21.97 mg/cm^2 foil

E_p (Mev)	$\frac{d\sigma}{d\Omega}(\gamma_0)$	$\frac{d\sigma}{d\Omega}(\gamma_1)$
6.3 ± 0.55	6.3 ± 1.0	5.1 ± 1.0
8.6 ± 0.4	8.0 ± 0.9	14.6 ± 1.5
8.9 ± 0.4	7.7 ± 1.4	17.8 ± 1.8
9.2 ± 0.4	6.2 ± 0.7	14.3 ± 1.4
10.4 ± 0.35	5.5 ± 0.7	13.7 ± 1.4
11.1 ± 0.35	3.2 ± 0.5	12.3 ± 1.2
11.5 ± 0.35	2.2 ± 0.4	10.8 ± 1.1
12.2 ± 0.3	2.0 ± 0.4	7.0 ± 1.1
12.7 ± 0.3	1.7 ± 0.5	5.5 ± 0.7
12.8 ± 0.3	1.8 ± 0.3	5.4 ± 0.9

Run 3: 5×6" crystal
22.17 mg/cm^2 foil

E_p (Mev)	$\frac{d\sigma}{d\Omega}(\gamma_0)$	$\frac{d\sigma}{d\Omega}(\gamma_1)$
5.2 ± 0.65	1.05 ± 0.3	3.1 ± 0.2
6.0 ± 0.55	4.15 ± 0.4	5.1 ± 0.5
6.6 ± 0.55	8.3 ± 0.8	7.7 ± 1.7
6.8 ± 0.5	5.0 ± 0.6	6.8 ± 0.4
7.2 ± 0.5	5.9 ± 0.6	7.6 ± 0.8
7.6 ± 0.45	5.4 ± 0.5	8.0 ± 0.8
8.2 ± 0.45	7.2 ± 0.7	8.3 ± 0.8
8.7 ± 0.45	8.5 ± 0.9	12.0 ± 1.2
9.0 ± 0.4	6.8 ± 0.7	13.1 ± 1.3
9.7 ± 0.4	7.6 ± 0.9	13.5 ± 1.5

IV. DISCUSSION

A. Resonance Behavior

It is clear from Fig. 10 that the 90° excitation functions for both γ_0 and γ_1 display the giant resonance behavior. The γ_0 curve appears to peak at a proton energy of about 9 Mev ($E_{\gamma_0} \approx 20$ Mev) and has a full width at half maximum of about 5 Mev. The γ_1 resonance, however, occurs at a higher proton energy. From Fig. 10, $E_m(\gamma_1) \approx 10$ Mev and $\Gamma(\gamma_1) \approx 4.5$ Mev. This upward shift in the peak position of γ_1 is also evident from the measurements of Gove[1] on the $B^{11}(p,\gamma)C^{12}$ reaction.

It should be pointed out that the Wilkinson model predicts the observed giant resonance behavior of γ_1 and can explain in a qualitative sense the energy shift noted above. The inverse of the $Al^{27}(p,\gamma_1)Si^{28*}$ reaction would be the (experimentally unrealizable) $Si^{28*}(\gamma,p_0)Al^{27}$ reaction. If the first excited state configuration of Si^{28} involves the rearrangement of only a few valence nucleons, then the bulk of the single-particle transitions responsible for the dipole absorption would be relatively unaffected, and the absorption behavior would be similar to that of Si^{28} in its ground configuration. In order to decay to the ground state of Al^{27}, however, the proton excited from the core must absorb the excitation energy (1.78 Mev in the case of Si^{28}), thus shifting the resonance up in energy by this amount. The different potential generated by the excited state configuration may, on the other hand, change the position of the single-particle levels responsible for the absorption. Thus the upward shift of Q(excitation) should be only approximately correct.

The fine structure exhibited by both curves was also observed by Gove. It has been noted by Wilkinson that this behavior is to be expected from the viewpoint of the independent particle model.[13] In contrast, the earlier collective model would predict a smooth resonance curve.

B. Angular Distributions

The γ_0 angular distribution (see Fig. 11) is isotropic, within statistics, while that for γ_1 appears to be asymmetric, falling off at the back angles. These measurements were taken at E_p = 8.7 Mev which corresponds to the main peak of the γ_0 resonance. The spread in proton energy, due to the foil thickness, was 0.9 Mev.

The form of the angular distributions expected from direct capture processes was first worked out by Courant[18] and can be derived easily from angular correlation theory. Pure f-wave absorption takes the form $1 + \sin^2\theta$ while p-wave absorption is given by $1 + (1/6)\sin^2\theta$. The latter possibility is favored (at E_p = 9 Mev) by about a factor of 3 from barrier penetration considerations. However, it has been pointed out by Eichler[21] that interference effects can modify the form of the angular distributions, which may account for the apparent isotropy of the γ_0 angular distribution. A detailed treatment should also consider the averaging effect of the finite source (foil) thickness.[13]

C. The Photoeffect in Si^{28}

A detailed balance calculation was carried out on the γ_0 data. For this purpose the smooth curve drawn through the γ_0 points in Fig. 10 was used and the assumption was made that $\sigma(p,\gamma_0) = 4\pi \frac{d\sigma}{d\Omega}(90°)$. In view of the angular distributions measured in this experiment

and those previously measured at lower energies by Gove,[1] this assumption is not too unreasonable. The Si^{28} $(\gamma,p_0)Al^{27}$ excitation function resulting from this calculation is presented in Fig. 12.

For the Si^{28} nucleus, the dipole sum rule gives σ_{int}(absorption) = 0.42 Mev-barn for a lower limit. Measurements by Johansson[2] on the integral yield of photoprotons gave $\sigma_{int}(\gamma,p)$ = 0.27 Mev-barn, while $\sigma_{int}(\gamma,n)$ has been found to be 0.07 Mev-barn.[6] For comparison, an integration over the Si^{28} $(\gamma,p_0)Al^{27}$ resonance of Fig. 12 yields $\sigma_{int}(\gamma,p_0)$ = 0.10 Mev-barn. Thus it appears that $\sim 1/4$ of the total absorption and fully 1/3 of the photoproton production in Si^{28} proceeds via the (γ,p_0) mechanism.

This rather large proportion of maximum energy protons seems incompatible with a purely statistical decay mode. Neutron evaporation takes the form $n(E) \propto Ee^{-E/T}$ where T represents the nuclear temperature. Although a proton decay spectrum would have a different shape, due to Coulomb effects which tend to shift the peak of the evaporation spectrum to higher energies, maximum energy decays would still be extremely improbable. It does not appear possible to understand the observed results with this mechanism.

On the other hand, the resonance-direct reaction mechanism offers a lucid explanation of the experimental results. By the use of Tables I and II a list of possible absorption transitions was compiled, with the percentage contribution of each transition to the total absorption cross section given in parentheses.

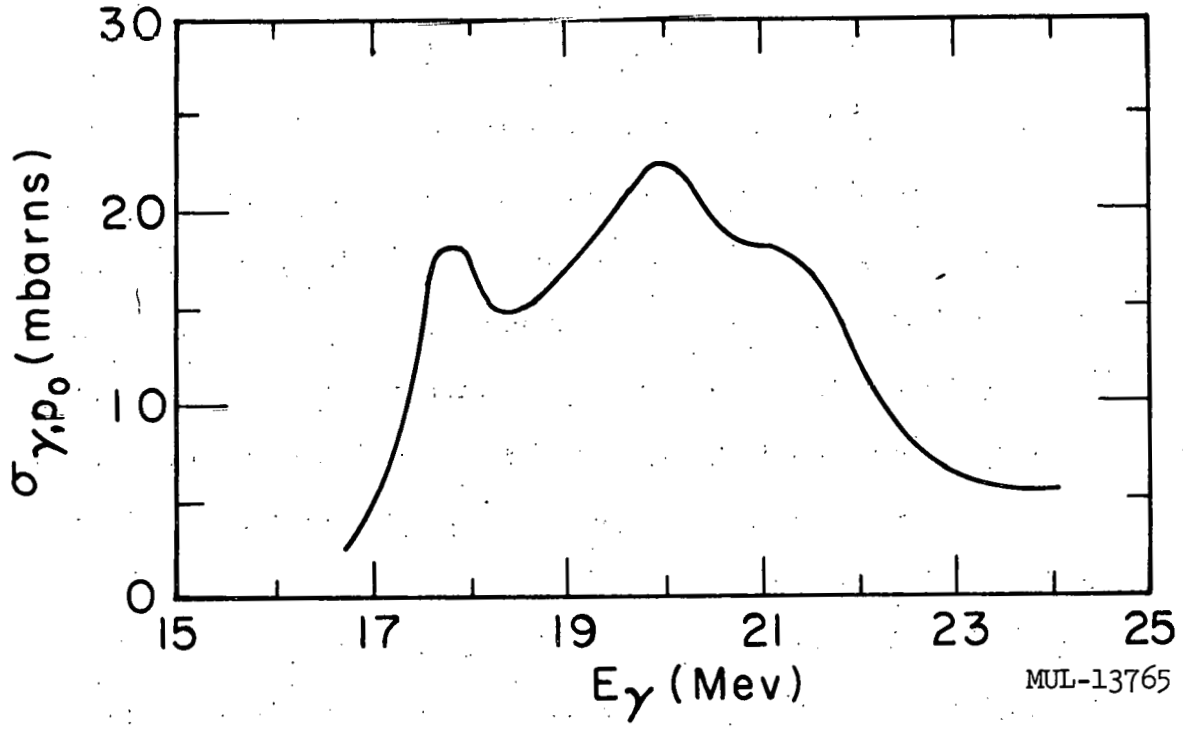

Fig. 12. $Si^{28}(\gamma,p_0)Al^{27}$ excitation function from detailed balance.

Transition	%
$1d_{5/2} \rightarrow 1f_{5/2}$	(3.6)
$1d_{5/2} \rightarrow 1f_{7/2}$	(72.3)
$1d_{5/2} \rightarrow 2p_{3/2}$	(8.0)
$1p_{1/2} \rightarrow 1d_{3/2}$	(8.1)
$1p_{1/2} \rightarrow 2s_{1/2}$	(1.0)
$1p_{3/2} \rightarrow 1d_{3/2}$	(3.2)
$1p_{3/2} \rightarrow 2s_{1/2}$	(3.8)

Noting that only the first three transitions (those from the uppermost or $d_{5/2}$ subshell) result in the concentration of the entire excitation energy in a single nucleon, it is clear that the $1d_{5/2} \rightarrow 1f_{7/2}$ transition should contribute the bulk of the ground-state reaction. Si^{28}, however, is a self-conjugate nucleus (N = Z), which implies equal effective charges for both neutrons and protons. Thus 1/2 of the table value or about 36% of the absorptions result in a proton being raised from the $d_{5/2}$ to the $f_{7/2}$ subshell.

Using the expression $\sigma = \sigma'(\Gamma/2W)$ implied by the simple form of the Wilkinson model, an estimate can now be made of $\sigma_{int}(\gamma,p_0)$. From the above considerations, $\sigma' = 0.36\sigma_{int}(\text{absorption}) \cong 0.15$ Mev-barn. Γ can be determined from the formula[15] $\Gamma = (2k\hbar^2/MR)T$, where T represents the barrier penetration probability for f-wave protons, k is the wave number of the emitted proton, M is the proton mass, and R is the effective radius[22] of Al^{27}. By means of the formulation of Weisskopf[23] and the exact Coulomb wave functions tabulated by Bloch,[24] T was calculated for 9-Mev protons, (corresponding to the peak of the γ_0 resonance) to be 0.2. With an assumed real well depth of 30 Mev,

it is found that $\Gamma \approx 2W \approx 3$ Mev.[15] Thus it is clear that $\Gamma/2W \approx 1$ and $\sigma_{int}(\gamma,p_0) \approx 0.15$ Mev-barn, essentially in agreement with the results of this experiment.

It should be emphasized that this prediction is an estimate only and cannot be taken too seriously. A detailed theoretical analysis has been made only for O^{16} and Ca^{40}, and unfortunately does not appear possible for other nuclei at present.[25,26] Even with the rather crude assumptions of the simple theory however, the agreement must be considered as strong evidence for the resonance-direct mechanism.

ACKNOWLEDGMENTS

The advice and collaboration of Dr. P. C. Gugelot has been an invaluable part of this experimental work and is sincerely appreciated. The early guidance of Dr. J. M. Peterson and the interest of Dr. Hans Mark in the latter stages of the experiment were also very helpful. I am indebted to Dr. John D. Anderson for many interesting and helpful discussions during the course of this work.

Special mention should be made of the competent help given by the various support groups associated with "P" Division at Livermore. The cooperation and help of Mr. Donald Rawles was especially valuable. Many other individuals too numerous to mention here were instrumental in bringing this work to a conclusion; their help is gratefully acknowledged.

This work was performed at the Lawrence Radiation Laboratory at Livermore under the auspices of the U. S. Atomic Energy Commission.

REFERENCES

[1]H. E. Gove, A. E. Litherland, and R. Batchelor, Phys. Rev. Letters 3, 177 (1959).

[2]Sven A. E. Johansson, Phys. Rev. 97, 1186 (1955).

[3]M. E. Toms, Bibliography of Photonuclear Reactions (Naval Research Laboratory, Washington, D. C.)

[4]D. C. Peaslee and V. L. Telegdi, Phys. Rev. 92, 126 (1953).

[5]J. J. DeSwart and R. E. Marshak, Phys. Rev. 111, 272 (1958).

[6]R. Montalbetti, L. Katz, and J. Goldemberg, Phys. Rev. 91, 659 (1953).

[7]R. Nathans and J. Halpern, Phys. Rev. 93, 437 (1954).

[8]J. S. Levinger, Ann. Rev. Nuclear Sci. 4, 13 (1954).

[9]L. Katz and A. G. W. Cameron, Can. J. Phys. 29, 518 (1951).

[10]K. L. Brown and R. Wilson, Phys. Rev. 93, 443 (1954).

[11]J. S. Levinger and H. A. Bethe, Phys. Rev. 78, 115 (1950).

[12]M. Goldhaber and E. Teller, Phys. Rev. 74, 1046 (1948).

[13]D. H. Wilkinson, Ann. Rev. Nuclear Sci. 9, 1 (1959).

[14]D. H. Wilkinson, Proc. Conf. Nuclear Meson Phys. Glasgow, 1954, 161 (1954).

[15]D. H. Wilkinson, Physica, 22, 1039 (1956).

[16]S. Rand, Phys. Rev. 107, 208 (1957).

[17]Proceedings of the International Conference on Nuclear Structure; Kingston, Canada (University of Toronto Press, Toronto, 1960), p. 539.

[18]E. D. Courant, Phys. Rev. 82, 703 (1951).

[19]Description in literature available from Harshaw Chemical Co., Cleveland, Ohio.

[20]J. Kokum and N. Starfelt, Nuclear Instr. and Methods 4, 171 (1959).

[21]J. Eichler and H. A. Weidenmuller, Z. Physik 152, 261 (1958).

[22]J. M. C. Scott, Phil. Mag. 45, 441 (1954).

[23]J. M. Blatt and V. F. Weisskopf, Theoretical Nuclear Physics (John Wiley and Sons, Inc., New York, 1952), p. 360.

[24]J. Bloch, M. M. Hull, Jr., A. A. Broyles, W. G. Bouricius, B. E. Freeman, and G. Breit, Revs. Modern Phys. 23, 147 (1951).

[25]J. P. Elliot and B. H. Flowers, Proc. Roy. Soc. (London) A242, 57 (1957).

[26]G. E. Brown, L. Castillejo, and J. A. Evans, Nuclear Phys. 22, 1 (1961).

/dr